Biogeosciences Open Access
Discussions
EGU

1 **A mechanistic model for electrical conduction in soil-root continuum: a virtual rhizotron**
2 **study**

3 Sathyanarayan Rao[1], Félicien Meunier[2], Solomon Ehosioke[3], Nolwenn Lesparre[4], Andreas
4 Kemna[5], Frédéric Nguyen[3], Sarah Garré[6], Mathieu Javaux[1,7].

5 [1] Université catholique de Louvain, Earth and Life Institute-Environmental Sciences, Louvain-la-
6 Neuve, Belgium
7 [2] Computational and Applied Vegetation Ecology lab, Ghent University, Gent, Belgium
8 [3] Applied Geophysics, Université de Liège, Chemin des Chevreuils 1, 4000 Liege, Belgium
9 [4] Laboratoire d'Hydrologie et Géochimie de Strasbourg, University of
10 Strasbourg/EOST/ENGEES, CNRS UMR 7517, 1 Rue Blessig, 67084 Strasbourg, France
11 [5] Department of Geophysics, University of Bonn, Meckenheimer Allee 176, 53115 Bonn,
12 Germany
13 [6] Université de Liège, Gembloux Agro-Bio Tech, TERRA Research and Teaching Center,
14 Passage des déportés 2, 5030 Gembloux, Belgium.
15 [7] Agrosphere, IBG3, Forschungszentrum Juelich GmbH, Germany
16
17 Correspondence to : Mathieu Javaux (mathieu.javaux@uclouvain.be)
18

19 **Abstract**

20 Electrical Resistivity Tomography (ERT) has become an important tool to study soil water fluxes
21 in cropped field. ERT results translates to water content via empirical pedophysical relations that
22 take soil physical properties into account, usually ignoring the impact of roots. Studies shows high
23 root dense soils behaves quite differently than less root dense soils in terms of bulk electrical
24 conductivity. Yet, we do not completely understand the impact of root segments on the ERT
25 measurements. In this numerical study, we coupled an electrical model with a plant-soil water flow
26 model to investigate the impact of plant root growth and water uptake on the ERT virtual
27 experiment. The electrical properties of roots were explicitly accounted in the finite element mesh
28 and we obtained the electrical conductivities of root segments by conducting specific experiments
29 on real maize plants. The contrast between electrical conductivity of roots and soil depends on
30 factors such as root density, irrigation, root age, and root water uptake pattern. Root growth and
31 water uptake processes thus affect this contrast together with the soil electrical properties. Model
32 results indicate a non-negligible anisotropy in bulk electrical conductivity induced by root
33 processes. We see a greater anisotropy in a sandy medium when compared to a loamy medium.
34 We find that the water uptake process dominates the bulk electrical properties. The Gauss-Newton
35 type ERT inversion of virtual rhizotron data demonstrate that, when root-soil electrical
36 conductivity contrasts are high, it can lead to error in water content estimates since the electrical
37 conductivity is partly due to root. Thus, incorporating the impact of root in the pedophysical
38 relations is very important to interpret ERT results directly as water content.
39

40

41

42

1 Introduction

Understanding root water uptake and associated nutrients is critical for crop management (e.g. Gregory et al. 2005) but remains a challenging task due to the inherent difficulty to collect observations in the soil (e.g. de Dorlodot et al., 2007). Geophysical monitoring of soil-root system water fluxes have received growing interest in the past decades to tackle this challenge. In particular, in this paper, we will particularly investigate the potential of Electrical Resistivity Tomography (ERT) (Michot et al., 2003; Paglis, 2013). This method aims at retrieving the 2D or 3D distribution of the electrical conductivity (σ) or its inverse resistivity in the soil. The electrical conductivity is then related to the variable of interest (for instance the soil water content SWC) through a pedophysical or petrophysical relationships.

In cropped fields, ERT method has been increasingly used for monitoring soil water content (SWC) (Beff et al., 2013; Brillante et al., 2016; De Carlo et al., 2015; Garrè et al., 2011; Michot et al., 2003; Srayeddin and Doussan, 2009; Vanella et al., 2018). More recently, ERT-estimated water content was used for phenotyping root systems at field scale (Whalley et al., 2017). The authors monitored changes in σ of the soil root zone in drying condition at different soil depths, which acted as a proxy of root activity. However, apparent or bulk conductivity of a vegetated soil (potentially containing roots), denoted by σ_{bulk}, is not only dependent to SWC but also to roots and their impact on soil structure. Field experiments further show that the rooted zone soil behaves quite different in terms of pedophysical relation as compared to soil containing no roots (Michot et al., 2016; Werban et al., 2008). Therefore ERT-monitored SWC in agricultural fields can be inaccurate or misleading if we ignore the impact of root-related processes on the bulk conductivity of the soil-root continuum.

In the literature, various studies mention or even target the impact of roots on σ_{bulk}. In Fig. 1, we report values of bulk soil electrical conductivity without roots, denoted by $\sigma_{bulk-soil}$, and root segment electrical conductivity, denoted by σ_{root}. The ratio between σ_{root} and $\sigma_{bulk-soil}$ is generally a function of plant species, soil type, SWC and solute concentration.

For a given species, σ_{root} is a function of root anatomy, which can be related to root age, root order or root diameter. In their study, Anderson and Higinbotham (1976), found that older maize root segments are electrically more conductive than younger roots. Their study was performed on excised root segments. They showed that the outer layer of the root segment (cortex) has very low

73   electrical resistance (~50 kΩ) in the radial direction when compared to the axial direction (~600

74   kΩ). By treating cortex and stele as concentric parallel conductors, the reported resistances, when

75   converted into conductivity are of the order σ_{root} ~ 0.05 S/m. However, the electrical behavior of

76   intact root segments embedded in the soil might be different as compared to excised segments.

77   Another study by Cao et al. (2010) reported that the root electrical resistance could be related to

78   root properties such as surface area, number of lateral roots and root length. Studies on poplar roots

79   show that σ_{bulk} of the soil-root medium may increase or decrease with the increase in root mass

80   density depending on the age of the plant (Al Hagrey, 2007; Zenone et al., 2008). On the other

81   hand, $\sigma_{bulk-soil}$ depends on several factors, the most important being the porosity of the soil, the

82   electrical conductivity of the soil fluid (σ_w), and SWC. In addition, loamy and clayey soils have a

83   surface conductivity that depends on mineral composition, SWC and σ_w (Friedman, 2005).

84   Literature on root electrical properties (Anderson and Higinbotham, 1976; Cao et al., 2010, 2011;

85   Ginsburg and Laties, 1973; Paglis, 2013) and pedophysical models for soils (Al Hagrey, 2007;

86   Amente et al., 2000; Bhatt and Jain, 2014; Friedman, 2005; Garrè et al., 2011; Laloy et al., 2011;

87   Werban et al., 2008; Wunderlich et al., 2013) suggest that if the contrast between σ_{root} and

88    $\sigma_{bulk-soil}$ is large enough, roots could have a measurable impact on ERT inversion results. In

89   addition there are studies that found a correlation between root length/mass density and electrical

90   resistivity obtained from ERT (Amato et al., 2009; Rossi et al., 2011). These studies used

91   destructive methods to determine root length density and root biomass. However, to our

92   knowledge, there are no detailed modeling efforts to study the effects of roots on electrical

93   conductivity of the bulk medium when monitoring SWC in cropped fields using the ERT method.

94   Beyond the impact of the electrical conductivity of root tissues, root-related processes like water

95   uptake, exudation or solute uptake will also affect the electrical properties of the rhizosphere, i.e.

96   the soil zone in close proximity to root segments, thereby affecting the σ_{root} - $\sigma_{bulk-soil}$ contrast.

97   The evolution of plant transpiration and root growth will also constantly impact the σ_{root} -

98    $\sigma_{bulk-soil}$ patterns. Recent ERT experiments on orange orchards field suggest that ERT results are

99   more sensitive to root water uptake pattern (Vanella et al., 2018) than the presence of resistive

100   lignified roots. While this may be true for orange trees, we need a thorough study to investigate the

101   sensitivity of ERT result on the presence of different types of root that are more electrically

102   conductive than soil. Therefore, to investigate the impacts of roots on ERT derived SWC, we

103   should take into account the root water uptake, soil heterogeneity, root specific electrical property

104   along with root growth.

105   To validate and quantify the impact of roots on ERT-derived SWC, we propose to simulate ERT

106   on a virtual soil-root system. Al Hagrey and Petersen (2011) studied the impact of roots on ERT

107   imaging by using a root growth model (Wilderotter, 2003), however they ignored the inherent

108   heterogeneity of σ_{root} and $\sigma_{bulk-soil}$. To understand the effect of root system connectivity and their

109   impact on SWC on σ_{bulk}, a model where roots are explicitly represented is needed. Explicit root

110   representation using unstructured finite element mesh has been studied for water and nutrient

111   uptake processes (Tournier et al., 2015; Wilderotter, 2003), but to the best of our knowledge, no

112   such work exists for ERT simulations coupled to a plant-soil water flow model.

113   The objective of this study is to investigate how a transpiring growing plant might affect the ERT

114   estimate of SWC. We hypothesize that the σ contrast between the plant root system and the soil

115   surrounding the roots (impacted by root, soil properties, and plant hydraulic boundary conditions)

116   together with the amount of roots will affect the ERT measurements and therefore ERT-derived

117   quantities. In our work, we model the electrical conductivity of the soil-root system in a rhizotron

118   geometry with a fine spatial resolution for the roots using an unstructured mesh for the ERT

119   simulation. The root model includes transient transpiration, root growth and root and soil water

120   redistribution. We choose the maize root system for our study and exclude root exudation and

121   solute uptake processes. We also study anisotropy in the electrical conductivity induced by root

122   growth and the water depletion pattern. An accurate electrical conductivity model of the soil-root

123   system will improve our understanding of the electrical behavior of the soil-root zone and hence

124   will help us in improving the ERT method as a feasible and faster tool to monitor soil moisture in

125   vegetated land. This study is therefore a first step towards a thorough understanding of the impact

126   of roots on SWC monitoring using the ERT method.

127   **2 Materials and Methods**

128   Our numerical experiment consists in running a combination of highly detailed simulations

129   representing the soil water fluxes in a planted 2-D rhizotron along with an ERT simulation. Root

130   and soil electrical and hydraulic properties were explicitly accounted for and spatially distributed

131   with a high resolution to study how root architecture and water uptake influence the ERT imaging

132   results and the interpretation in terms of SWC. Fig. 2 summarizes the various steps described below

133   in a flow diagram.

2.1 Rhizotron/plant water flow model

135   A two-dimensional root architecture was extracted from light transmission experiments on a real

136   rhizotron with a 21 days old maize species using the root image analyzing tool SMARTROOT

137   (Lobet et al., 2011). The digitized root (see Fig.3) was then used for root water uptake modeling

138   using R-SWMS (Javaux et al., 2008). Since the root growth was monitored every day, ages were

139   easily assigned to each root segment. Root growth was simulated by updating the root system

140   architecture at each time step between the beginning (day 5) and the end (day 22) of the simulation.

141   Cyclic transpiration demand was imposed as top boundary condition for the root system. The daily

142   transpiration was supposed to linearly increase between the root emergence and the end of the

143   study. At day 22, daily transpiration reached 25 cm³.

144   The root system is entirely contained in soil box whose length, thickness and depth were 22 cm, 1

145   cm, and 40 cm respectively (the corresponding reference axes are -11< x< 11cm, -0.5<y<0.5 cm,

146   -40<z<0 cm). In the scenario analysis, we considered both sandy and loamy soil types whose

147   hydraulic properties were supposed to be perfectly represented by Mualem-van Genuchten

148   equations (van Genuchten, 1980). Hydraulic parameters for both soils are given in Table 1.

149   The initial soil condition was a hydrostatic equilibrium with a saturated soil at the bottom of the

150   rhizotron and root transpiration was the only source/sink term that allowed the total water content

151   to change. R-SWMS (Javaux et al., 2008) uses the finite element method on a regular uniform grid

152   to solve Richards equation in order to simulate three-dimensional water flow in the soil:

153    $$\frac{\partial \theta}{\partial t} = \frac{\partial}{\partial x}\left(K\frac{\partial h}{\partial x}\right) + \frac{\partial}{\partial y}\left(K\frac{\partial h}{\partial y}\right) + \frac{\partial}{\partial z}\left(K\frac{\partial (h+z)}{\partial z}\right) - Sink \qquad [1]$$

154   ,where θ is the volumetric SWC, h the matrix head, K the isotropic hydraulic conductivity, $Sink$

155   is a sink term for root water uptake [cm^3 cm^{-3} day^{-1}], and x,y and z are the spatial coordinates.

156   Experimentally measured maize root hydraulic conductivities were used in the R-SWMS model,

157   in which they are age and type dependent (Couvreur et al., 2012; Doussan et al., 2006). Two-

158   dimensional distributions of roots and of SWC were subsequently transformed into electrical

159   conductivity maps through appropriate bio-pedo electrical relations.

Biogeosciences
Discussions

160 **2.2 Electrical properties of plant root tissues and soils**

161 To get insight into maize root electrical properties, we designed specific experiments on intact root

162 segments (Ehosioke et al., in preparation). First, we identified and separated the primary and brace

163 roots from maize plants grown in laboratory and were thoroughly washed with demineralized water

164 and dried with absorbent tissue. The electrical resistance of root segments was measured using a

165 digital multimeter and were converted into electrical conductivity (σ_{root}) by approximating the

166 root segment as a cylindrical geometry similar to Cao et al. (2010). The measurement direction of

167 root segments in Cao et al. (2010) is from root apex towards root collar while it is opposite in the

168 case of our experiment. We studied intact root segments as compared to excised root segments in

169 the studies of Cao et al. (2010) or Anderson and Higinbotham (1976) and investigated both primary

170 and brace roots in the experiments. We examined variations of σ_{root} with respect to the segment

171 distance from the root collar and root cross-sectional area with a segment length of 4 cm.

172 Conductivity gel (*Rodisonic*, from Pannoc Nv/SA Belgium) was used to improve the electrical

173 contact between root segments and measuring electrodes,. However, in the simulation model, only

174 the variations of σ_{root} as a function of segment distance from the root collar is used. The digital

175 maize roots in our simulation are around three weeks old while the brace roots develop only after

176 several weeks in a real maize plant; hence, the brace root data are not included in our model.

177 To compute soil electrical properties, we used Archie's law (Archie, 1942) with an additional term

178 for surface conductivity of the solid phase $\sigma_{surface}$, which is assumed to act in parallel (Waxman

179 and Smits, 1968). The relation between soil water content θ and σ_{soil} for unsaturated soil is given

180 by Eq. 2, where Archie's fitting parameters (m and d) vary for different types of soil (Friedman,

181 2005):

182 $$\sigma_{bulk-soil} = \sigma_w n^m S^d + S^{d-1} \sigma_{surface}, \qquad [2]$$

183 where, S is the degree of water saturation ($S = \frac{\theta}{n}$), n the porosity of soil (assumed to be equal to

184 saturated water content: θ_s), $\sigma_{bulk-soil}$ the bulk electrical conductivity of the soil medium without

185 considering roots (more specifically, $\sigma_{bulk-loam}$ for loam and $\sigma_{bulk-sand}$ for sand), σ_w the

186 conductivity of soil fluid phase, $\sigma_{surface}$ is the surface electrical conductivity of the solid phase of

187 the soil. Sand typically has very low surface conductivity ($\sim 10^{-5} \ S/m$) while for loam, we assume

188 $\sigma_{surface}$ to be 0.015 S/m (Brovelli and Cassiani, 2011). For Archie's fitting parameters, we use the

189   typical values d = 2 and m =1.3 (e.g. Werban et al., 2008). $\sigma_{bulk-soil}$, in the rhizotron also depends

190   on the electrical conductivity of the nutrient solution (σ_w) in the rhizotron used to grow plants.

191   Measurements from suction cups indicate that σ_w varies between 0.06 to 0.2 S/m (Jougnot et al.,

192   2012). We assume σ_w to be 0.2 S/m and choose n as 0.35 (sand) and 0.435 (loam), respectively,

193   for calculating and comparing different pedophysical models. In the following sections, we will

194   refer $\sigma_{bulk-soil}$ the soil bulk electrical conductivity (with $\sigma_{bulk-loam}$ and $\sigma_{bulk-sand}$ to specify

195   soil type) when no roots are present and σ_{bulk} will be used for studies or dataset where both roots

196   and soil are present.

197   **2.3 Electrical modeling in EIDORS**

198   The ERT forward problem seeks apparent conductivity or voltage data by solving the Poisson's

199   equation with appropriate boundary conditions with a known electrical conductivity distribution.

200   In ERT inverse problem, we aim at reconstructing an estimate of the electrical conductivity

201   distribution within the soil-root domain from apparent conductivity or voltage measurements at its

202   boundary or at some discrete locations within the computational domain. The inverse problem finds

203   an approximate σ-distribution that minimizes the data misfit between the virtual measurements and

204   the model predictions in a least-square sense in addition to a regularization term. We use the finite-

205   element based software EIDORS (Adler and Lionheart, 2006) to solve the forward and inverse

206   problems as it offers flexibility in using different meshing software such as NETGEN (Schöberl,

207   1997) and gmsh (Geuzaine and Remacle, 2009). The integration of such meshing software allows

208   creating complex finite-element models for electrical conduction in a soil-root medium. The

209   electrical conduction model for the rhizotron is in purely 2-D (x-z plane, y=0). A point electrode

210   model (Hanke et al., 2011) with a total number of 50 electrodes and a dipole-dipole measurement

211   scheme is used to compute the forward response. All the electrodes are located at the boundary of

212   the computational domain with a similar set-up as in Weigand and Kemna (2017). Three different

213   finite-element meshes are used (Fig. 4). To simulate the ERT data set, the root growth simulation

214   model mesh (SMDL), with an explicit representation of the root architecture is used. The ERT

215   forward model mesh (FMDL), which does not contain the root architectural information, is used

216   to compute the data misfit in the ERT inversion, and the ERT inverse mesh, a comparatively coarse

217   mesh is used to compute the Jacobian in the ERT reconstruction. In the SMDL, either a σ_{root} or

218    $\sigma_{bulk-soil}(\theta)$ value is assigned to each element. The maize primary roots in our simulation have a

219   mean thickness (~ 0.05 cm) which is small compared to the dimensions of rhizotron (20x40 cm),

220   requiring a very high spatial resolution for roots in the SMDL.

221   To generate a root resolved mesh with high spatial resolution, first we created the binary images

222   of root architectures at various ages (day 5, 7, 10, 12, 15, 18, 22, see Fig. 3). In these binary images,

223   we removed extremely fine root hairs and root branches that were below 0.01 cm in thickness,

224   assuming that such roots have negligible effect on the electric potential distribution. The simplified

225   root image represent root branches with a mean diameter of 0.05 cm. First, we convert binary image

226   into a spline function that traces the boundary of the root surface (red lines in Fig. 4 b) using the

227   boundary tracing function "bwboundaries" in MATLAB. The spline function representing the root

228   shape was converted into finite element mesh using gmsh software. The root architecture mesh

229   created in this manner possesses superior quality in terms of aspect ratio of elements and is

230   computationally efficient. We then solved the electrical forward problem for the generated σ-map

231   yielding virtual ERT data, which is subsequently inverted using EIDORS. For the inversion, first

232   we generate a forward data set (d_1) for a homogeneous σ-distribution ($\sigma_1 = 1\ S/m$). Then the

233   second forward data d_2 is computed using SMDL filled with σ_1 in addition to soil-root electrical

234   conductivity distribution ($\sigma_2 = \sigma_1 + \sigma_{bulk}$). A difference ERT inversion Gauss-Newton (GN) one

235   step algorithm is used to estimate the change in the conductivity ($\delta\sigma = \sigma_2 - \sigma_1$) from the change

236   in measurements ($\delta d = d_2 - d_1$) (Adler et al., 2007). The inversion is regularized using a

237   Laplacian matrix. We assume a low noise data set and hence δd is added with 1% random noise

238   proportional to each measurement. The FMDL mesh is used to compute the ERT data (δd) and the

239   data misfit while the inverse mesh is used for the GN inversion.

240   **2.4 Computing average and effective electrical properties**

241   To get an insight on how a rooted soil might differ from bare soil pedophysical model (Eq. 2), we

242   compare bulk electrical conductivity of soil-root medium, at two different scales: 2x2 cm and 20 x

243   40 cm.

244   At smaller scale, the block-wise averaged data, denoted by $<\sigma_{bulk}>$ and $<\theta>$ for electrical

245   conductivity and water content respectively , are computed from averaging the corresponding data

246   in the simulation model finite element mesh with an averaging block size of 2cm x 2cm (see Fig.

247   7a). Averaging in each block is done by taking the arithmetic and the harmonic averages of

248   conductivity data of all finite elements within each averaging block to get $<\sigma_{bulk}>$. The arithmetic

249   averages assumes that the soil-root elements in each averaging block are connected in series while

250   the harmonic mean assumes the elements to be in parallel. For $\langle\theta\rangle$, we computed only the

251   arithmetic mean. In reality we expect, the real $\langle\sigma_{bulk}\rangle$ to be in between the arithmetic and

252   harmonic averages. The relation between the collection of averaged data points at every averaging

253   block and at all time (day 5 to , i.e. $\langle\theta\rangle$ vs $\langle\sigma_{bulk}\rangle$, will then approximately mimic the impact of

254   roots at a block-scale on σ_{bulk} , when compared to the Archie's law applied in soils only (Eq.2).

255   At larger scale (rhizotron scale, i.e. 20cm x 40 cm), simple mean of arithmetic and harmonic

256   averages over whole domain may not exactly represent bulk property, as we need to account the

257   complex structural variations of electrical conductivity distributions and heterogeneity in soil

258   electrical property. Hence, to compute σ_{bulk}, at the scale of the rhizotron, we solve the Poisson's

259   equation between two plate electrodes at the boundaries with root included (a root segment has its

260   own electrical conductivity) and without root. The computation is repeated for two directions: in

261   horizontal (σ_{bulkX}) and vertical direction (σ_{bulkZ}). We included in our simulations, the plate

262   electrodes that cover the entire left and right walls of the rhizotron as well as top and bottom wall

263   of rhizotron and the ratio of injected current to measured voltage in these electrodes with the

264   geometric factor considerations gives σ_{bulkZ} and σ_{bulkX}.

265   **3 Results**

266   **3.1 Electrical measurements on Maize root segments**

267   Figure 5a shows the experimental data of σ_{root} as a function of root age for Maize. We observe a

268   gradual increase in σ_{root} of intact maize root segments, as the segment distance from root collar

269   increased (Fig. 5a). The trend is different in primary and brace roots, where the brace root

270   conductivity increases much more rapidly with increasing distance of the segment from the root

271   collar compared to primary root segments. The σ_{root} also varies with respect to root cross-sectional

272   area. Our measurements indicate that thinner roots have higher σ_{root} compared to thicker roots

273   (Fig. 5b). This could be due to higher water content of younger roots. Since we measured intact

274   root segments, the surface electrical conductivity of endodermis and contact resistance of stele and

275   cortex layers of the root are accounted in the measurements. The thicker outer layer (cortex) of the

276   root is electrically more insulating than water rich younger roots or inner part (stele) as seen in

277   early studies of Anderson et al. (1976). However, our measurements represent the combined

278   resistivity of cortex and stele in an intact form. Age dependent electrical conductivity variations

279   within a given species were earlier studied in poplar roots (Zenone et al., 2008). Fig. 5a shows that

280   within the same species, in addition to age, different types of roots (brace and ground roots) can

281   have different electrical properties. However, in the modeling work, we do not consider the

282   development of brace roots as the simulated root system in the model is relatively young (3-weeks

283   old). The blue-curve of Fig. 5a represents the data incorporated in our simulations: 0.0154

284    $< \sigma_{root} < 0.03$ [S/m].

285   **3.2 Virtual root simulation**

286   Simulations show that the relative SWC distribution patterns depend on the soil type (Figs. 6 a, b).

287   After 22 days, the depletion is higher is the sand rhizotron as θ_s is lower. In the loam, the soil is

288   wetter and the contrast in saturation degree between the rooted and unrooted parts of the soil is

289   much bigger.

290   When translated into electrical conductivity maps including the root electrical properties, we see

291   different trends for sand and loam. For sand, we notice that σ_{root} is always larger than $\sigma_{bulk-sand}$

292   and the difference between σ_{root} and $\sigma_{bulk-sand}$ is always positive (Fig. 6c). For loam, however,

293   we see that different regions where σ_{root}- $\sigma_{bulk-loam}$, contrast changes with time (Fig. 6d). At

294   initial time, $\sigma_{bulk-loam}$ is larger than σ_{root} but at day 18, we see different regions, where the

295   difference between σ_{root} and $\sigma_{bulk-loam}$ is either positive, negative or close to zero. Such contrast

296   does not manifest in sand. At day 22, in the upper portion of rhizotron, σ_{root} is greater than

297    $\sigma_{bulk-loam}$ whereas in the lower portion of rhizotron, the roots are masked by $\sigma_{bulk-loam}$ (see Fig.

298   6d). In real scenarios, i.e in any soil-root system, there potentially exist three regions, where the

299   difference between σ_{root} and $\sigma_{bulk-soil}$ is either positive, negative or close to zero. In our study,

300   we observe that at low SWC, the mean of σ_{root} is greater than the mean of $\sigma_{bulk-loam}$ and at high

301   water content, the mean of σ_{root} is lower than the mean of $\sigma_{bulk-loam}$, while in sand, the mean of

302   σ_{root} is nearly same as the mean of $\sigma_{bulk-sand}$ (Fig. 6e). Since electric current flow depends on the

303   gradient of σ-distribution, the effect of roots in ERT experiments will be greater where there is

304   higher $\sigma_{root} - \sigma_{bulk-soil}$ contrasts and most importantly, it is time dependent (Fig. 6e). In addition,

305   the density of roots plays a role in terms of $\sigma_{root} - \sigma_{bulk-soil}$ contrasts, for instance at day 22, the

306   upper part of the root system is more conductive than $\sigma_{bulk-loam}$ in the upper part of the rhizotron

307   and also reflects higher root volume than at initial times. Therefore, at later times (Fig. 6d, day 22),

308   the ERT estimate of water content in the upper region could be misleading due to a stronger root

309   influence on σ_{bulk}.

3.3 Bulk electrical properties

The block wise averaged data shows that lower the root surface area, closer is the averaged data to the bare-soil pedophysical relation (Figs. 7 b and d). In sand, we see more difference between arithmetic and harmonic mean with harmonic mean staying closer to the original pedophysical curve than arithmetic mean (Fig. 7b). In loam, however, there is no big difference between arithmetic and harmonic block wise averaged data and both of them change the curvature of the pedophysical relation (Fig. 7d). As expected, when root density is high, the $<\theta>$ vs $<\sigma_{bulk}>$ plot significantly deviates from Eq. 2 and always overestimates $\sigma_{bulk-sand}$, whereas areas with very low to zero root density lie along $\sigma_{bulk-soil}(\theta)$ curve (blue dots on $\sigma_{bulk-soil}(\theta)$ curve for $\theta > 0.2$ in Fig. 7b and $\theta > 0.3$ in Fig. 7d). In loam, the $<\theta>$ vs $<\sigma_{bulk}>$ points are scattered around the petrophysical relationship with a tendency of both overestimating $\sigma_{bulk-loam}$ for $\theta < 0.2$ and underestimating $\sigma_{bulk-loam}$ for $\theta > 0.2$ in the root dense region. This illustrates how roots might affect the relationship between SWC and σ_{bulk}.

At rhizotron scale, the effective bulk property shows significant anisotropic affect in sand (notice the difference between σ_{bulkX} and σ_{bulkZ} in Fig. 7c). We expect that the dry sand act as a barrier to the electrical current flow, thereby decreasing the σ_{bulk}. The vertical direction has more pronounced anisotropy, when compared to horizontal direction ($\sigma_{bulkX} > \sigma_{bulkZ}$), as we see less deviation of σ_{bulkX} from Eq. [2] when compared to σ_{bulkZ}. This is due to horizontal layering that develops in the electrical conductivity distribution due to root water uptake, which thereby affects current more in vertical direction than in horizontal direction. For loam medium, the anisotropic effect is less when compared to sand. We see from the effective bulk properties that the original pedophysical relation (Eq. [2]) would rather under-estimate the water content in loam where as it would over-estimate in sand (Fig.7 c and e). Computed σ_{bulkX} and σ_{bulkZ} data points lie below $\sigma_{bulk-soil}(\theta)$ in sand medium whereas above in the loam medium. The rhizotron scale, bulk electrical conductivity deviates from Eq. [2] quite differently when compared to the averaged data at smaller scale. This can be understood as the impact of soil heterogeneity playing a bigger role in influencing the bulk property at large scale whereas at centimeter-scale (2cm x 2cm), the root density plays a major role in the deviating the bulk property from bare soil pedophysical relation (Eq.[2]).

339   Table 2 gives the computed anisotropy factor, $AF = \sigma_{bulkX}/\sigma_{bulkZ}$ for cases with and without

340   roots. As we can see from the table, the main anisotropic affect is due to soil heterogeneity and not

341   the root themselves.

3.5 ERT Inversion result

343   The GN type ERT inversion was performed on the virtual measurement data set from the forward

344   conductivity distribution with root system included (Figs. 8 a,d) and also without considering the

345   root system. Figures 8b and 8e shows the ERT inversion with root system included sand and loam

346   medium, respectively. As we can see, the inversion works well in recovering most of the important

347   features of soil water depletion, but sometimes we can observe contamination due to the presence

348   of roots (for example day 18 and 22 in Fig. 8b). Note that for sand the presence of roots increased

349   the electrical conductivity while for loam it decreased the electrical conductivity.

350   Figures 8c and 8f represents the difference in the inversion results of virtual data from forward

351   conductivity distributions with and without root systems. The inversion result with roots is showed

352   in Figs 8 (b and e) but the inversion results without considering the root system are not shown here.

353   They were realized by inverting the apparent resistance data resulting from the conductivity

354   distributions from soil water content map without the root electrical properties (but with the impact

355   of the root system on the SWC and not in electrical conductivity map). This difference maps

356   represent the impact of the roots on the ERT inverted σ-distributions (see Fig.8 c and f). In sand,

357   the error in estimating the electrical conductivity corresponding to the water content of Eq. [2] can

358   be as low as 2% when the roots are small and can reach up to 15% when soil becomes dry and

359   roots occupy the whole rhizotron.

360   By comparing Figs. 8(a,b,c) and 8 (d,e,f), we can immediately see that in loam, the contrast between

361   root and soil is low or the soil is more conductive than root at most time. Roots are like low

362   conductive wires in the loam medium surrounded by highly conductive soil. Since $\sigma_{bulk-loam}$

363   dominates the effective properties, the impact of roots is also lower in loam compared to that of

364   sand. At later time (Fig. 8d, day 22), as root water uptake becomes significant, the contrast between

365    $\sigma_{bulk-loam}$ and σ_{root} reduces making roots indistinguishable from soil. Figures 8c and 8f indicate

366   that the error in the estimation of the conductivity /water content increases with ongoing root

367   growth. While the error pattern is monotonic in sand increasing with root growth, in loam we see

368   different regions of high and low error depending on soil-root contrast. These errors in σ-estimate

369   manifest in the SWC estimated from Eq. [2]. We denote here, the volumetric average of water

370   content from RSWMS simulation by: θ_1, volumetric average of water content from ERT inverted

371   σ-map without the root electrical properties in the ERT forward data by: θ_2 , and volumetric

372   average of water content from ERT inverted σ-map with the root electrical properties included in

373   the ERT forward data by: θ_3. We show θ_1, θ_2 and θ_3 as a function of time in Figure 9 (a, d). The

374   difference between θ_1 and θ_2 is the error induced due ERT inversion procedure alone while the

375   difference between θ_1 and θ_3 is the error induced due to ERT method as well as the root segments.

376   In Figure 9 (b,c,e,f), we show that these errors in absolute and relative terms are more pronounced

377   when the root system is large. When the root is young (age <10), the absolute error between θ_1

378   and θ_2 is same as the absolute error between θ_1 and θ_3 indicating that root segments has no

379   significant impact in water content estimates (Fig. 9b and e).

380   **4 Conclusions**

381   We simulated an electrical conductivity model of a soil-root continuum in the rhizotron geometry.

382   The roots were explicitly represented in the σ-distribution and root water uptake was simulated

383   using mechanistic water flow models in soils and roots. We designed experiments on intact root

384   segments to measure electrical properties of roots (σ_{root}). Our measurements on maize root

385   segments indicated that σ_{root} is a function of distance from the root collar and root type (primary

386   and brace roots). We incorporated the distance variations of primary roots into our model based on

387   a polynomial fit.

388   Soil-root water flow modeling together with root electrical measurements reveals that soil-root

389   electrical conductivity contrasts changes over time (Fig. 6) as a function of soil type and root water

390   uptake. At centimeter-scale (2cm x 2 cm), the root play a major role in deviating σ_{bulk} from Eq.

391   [2]. Block-wise averaged data (<θ> vs <σ_{bulk}>) shows that rooted soil deviates in terms of

392   pedophysical relation from bare soil, where there is higher root density (Fig.7). This is consistent

393   with the experimental observation made by Michot et al., (2016), where they found that bare-soil

394   pedophysical relation is inadequate to explain $\sigma_{bulk}(\theta)$ in the rooted zone. At decimeter scale, the

395   σ_{bulk} computed using plate electrode reveals anisotropy and different behavior as compared to the

396   centimeter scale averaged data (see Fig. 7 b and c). We also observe an anisotropy factor of around

397   six for fully mature root systems. This is mostly due to water content distribution pattern induced

398   by root water uptake. At rhizotron scale, anisotropy is stronger in sand, when compared to loam,

399   and increases non-linearly with root growth (Table 2).

Biogeosciences
Discussions

400   The GN type ERT inversion results (Figs. 8) reveal that exclusion of the explicit representation of
401   roots in the forward model results in an error of 5 to 15% in σ. Even though the effect of roots at
402   rhizotron scale is not evident in the bulk property analysis of conductivity data (table 2), it is evident
403   in ERT inversion result. This indicates the importance of incorporating the effect of roots in the
404   pedophysical model. The volumetric total water content shows a larger error for sandy soil (Fig.9).
405   However, yet the overall trend of decrease in total water content due to root water uptake is
406   recovered. The difference ERT inversion algorithm works well in recovering the overall structure
407   of water uptake. For maize roots, the water uptake process dominates the σ-distribution of the soil-
408   root system as reconstructed with ERT. It is also worth noting that there are various other root
409   architectures such as tap root systems, which still need further investigations on their electrical
410   anisotropy at rhizotron scale and at field scale.

411   The modeling results clearly show that, roots impacts ERT results. The degree of impact further
412   depends on electrical conductivity contrast between root and soil. To characterize the specific
413   impact of roots in ERT monitored water content estimates, we need the knowledge of electrical
414   conductivity contrast between root and soil as a function of space and time. Estimating this contrast
415   between root and soil, however, is not so straightforward and difficult, as they are root type, root
416   age, root radius, soil type and water content dependent. Although the maize simulations in this
417   study indicates that water content is the dominant factor affecting bulk electrical conductivity, other
418   factors do play a role including the root connectivity that induces electrical anisotropy. Further
419   upscaling the electrical properties derived from centimeter scale (root segment) to decimeter scale
420   (rhizotron) to field scale (~100 meter) is very important to develop a proper pedophysical relation
421   that completely eliminates the root impact in the water content estimate.

422   Since our model indicates a non-negligible anisotropy factor in the electrical conductivity, ERT
423   injection scheme should consider exploiting them to retrieve better information, for example, by
424   having an injection scheme that maximizes the sensitivity in the region of anisotropy. Since
425   anisotropy in σ changes with development of the root system in soil, one could also have time-
426   dependent ERT injection schemes for the time-lapse ERT. A prior knowledge of time dependent
427   electrical conductivity contrasts between soil and root, for a given crop, can definitely help in
428   designing optimized ERT injection scheme for the future field experiments.

429   Finally, we considered a very limited range in $\sigma_{root} - \sigma_{bulk-soil}$ variability. In reality, the range

430   of variations in $\sigma_{root} - \sigma_{bulk-soil}$ could differ depending on the type of roots and the value of σ_w

431   (Fig.1). As in agricultural fields, even in two-dimensional rhizotron experiments, air filled cracks

432   can manifest in the soil, potentially influencing ERT measurements. In our model, we did not

433   consider such real-world phenomena and limited our study only to the impact of roots. We also

434   ignored rhizosphere processes such as root exudation, which could affect the water content

435   estimates. In reality, soil-root systems are three-dimensional structures and two-dimensional

436   rhizotron approximations may not represent an accurate model for three-dimensional electrical

437   conductivity in real soil-root environments (e.g. cropped fields). We also ignored the anisotropy of

438   σ inside the root structure (stele-cortex variations), which may have a considerable effect on ERT

439   measurements. Such structural variations may induce even higher degree of anisotropy in the

440   electrical conductivity. Our next step will be the validation of our findings in real experiments and

441   under even more realistic conditions, accounting, amongst other aspects, for the specific

442   rhizosphere properties, and to extend the studies to include complex conductivity (induced

443   polarization) properties.

444   **References**

445   Adler, A. and Lionheart, W. R. B.: Uses and abuses of EIDORS: an extensible software base for EIT,
446   Physiological Measurement, 27(5), S25, 2006.

447   Adler, A., Dai, T. and Lionheart, W. R. B.: Temporal image reconstruction in electrical impedance
448   tomography, Physiol. Meas., 28(7), S1, doi:10.1088/0967-3334/28/7/S01, 2007.

449   Al Hagrey, S. A.: Geophysical imaging of root-zone, trunk, and moisture heterogeneity, Journal of
450   Experimental Botany, 58(4), 839–854, doi:10.1093/jxb/erl237, 2007.

451   Al Hagrey, S. A. and Petersen, T.: Numerical and experimental mapping of small root zones using
452   optimized surface and borehole resistivity tomography, Geophysics, 76(2), G25–G35,
453   doi:10.1190/1.3545067, 2011.

454   Amato, M., Bitella, G., Rossi, R., Gómez, J. A., Lovelli, S. and Gomes, J. J. F.: Multi-electrode 3D resistivity
455   imaging of alfalfa root zone, European Journal of Agronomy, 31(4), 213–222,
456   doi:10.1016/j.eja.2009.08.005, 2009.

457   Amente, G., Baker, J. M. and Reece, C. F.: Estimation of Soil Solution Electrical Conductivity from Bulk Soil
458   Electrical Conductivity in Sandy Soils, Soil Science Society of America Journal, 64(6), 1931–1939,
459   doi:10.2136/sssaj2000.6461931x, 2000.

460   Anderson, W. P. and Higinbotham, N.: Electrical Resistances of Corn Root Segments, Plant Physiology,
461   57(2), 137–141, 1976.

462   Archie, G. E.: The Electrical Resistivity Log as an Aid in Determining Some Reservoir Characteristics, SPE-
463   942054-G, doi:10.2118/942054-G, 1942.

464   Beff, L., Günther, T., Vandoorne, B., Couvreur, V. and Javaux, M.: Three-dimensional monitoring of soil
465   water content in a maize field using Electrical Resistivity Tomography, Hydrol. Earth Syst. Sci., 17(2), 595–
466   609, doi:10.5194/hess-17-595-2013, 2013.

467   Bhatt, S. and Jain, P. K.: Correlation between electrical resistivity and water content of sand – a statistical
468   approach, Am. Int. J. of Res. in Sci., Tech., Eng. & Math., 6(2), 115–121, 2014.

469   Brillante, L., Bois, B., Lévêque, J. and Mathieu, O.: Variations in soil-water use by grapevine according to
470   plant water status and soil physical-chemical characteristics-A 3D spatio-temporal analysis, European
471   Journal of Agronomy, 77, 122–135, doi:10.1016/j.eja.2016.04.004, 2016.

472   Brovelli, A. and Cassiani, G.: Combined estimation of effective electrical conductivity and permittivity for
473   soil monitoring, Water Resour. Res., 47(8), W08510, doi:10.1029/2011WR010487, 2011.

474   Cao, Y., Repo, T., Silvennoinen, R., Lehto, T. and Pelkonen, P.: An appraisal of the electrical resistance
475   method for assessing root surface area, Journal of Experimental Botany, 61(9), 2491–2497,
476   doi:10.1093/jxb/erq078, 2010.

477   Cao, Y., Repo, T., Silvennoinen, R., Lehto, T. and Pelkonen, P.: Analysis of the willow root system by
478   electrical impedance spectroscopy, Journal of Experimental Botany, 62(1), 351–358,
479   doi:10.1093/jxb/erq276, 2011.

480   Couvreur, V., Vanderborght, J. and Javaux, M.: A simple three-dimensional macroscopic root water
481   uptake model based on the hydraulic architecture approach, Hydrol. Earth Syst. Sci., 16(8), 2957–2971,
482   doi:10.5194/hess-16-2957-2012, 2012.

483   De Carlo, L., Battilani, A., Solimando, D., Battilani, A., Lo Porto, A. and Caputo, M. C.: Monitoring different
484   irrigation strategies using surface ERT, pp. 71–75. [online] Available from:
485   https://www.scopus.com/inward/record.uri?eid=2-s2.0-
486   84957960460&partnerID=40&md5=d5a2e82335284345a7097045eaaad93b, 2015.

487   de Dorlodot, S., Forster, B., Pagès, L., Price, A., Tuberosa, R. and Draye, X.: Root system architecture:
488   opportunities and constraints for genetic improvement of crops, Trends in Plant Science, 12(10), 474–
489   481, doi:10.1016/j.tplants.2007.08.012, 2007.

490   Doussan, C., Pierret, A., Garrigues, E. and Pagès, L.: Water Uptake by Plant Roots: II – Modelling of Water
491   Transfer in the Soil Root-system with Explicit Account of Flow within the Root System – Comparison with
492   Experiments, Plant Soil, 283(1–2), 99–117, doi:10.1007/s11104-004-7904-z, 2006.

493   Ehosioke, S., Sarah Garré, Kremer, T., Rao, S., Kemna, A., Huisman, J., Zimmermann, E., Javaux, M. and
494   Nguyen, F.: A NEW METHOD FOR CHARACTERIZING THE COMPLEX ELECTRICAL PROPERTIES OF ROOT
495   SEGMENTS, n.d.

496   Friedman, S. P.: Soil properties influencing apparent electrical conductivity: a review, Computers and
497   Electronics in Agriculture, 46(1–3), 45–70, doi:10.1016/j.compag.2004.11.001, 2005.

498   Garrè, S., Javaux, M., Vanderborght, J., Pagès, L. and Vereecken, H.: Three-Dimensional Electrical
499   Resistivity Tomography to Monitor Root Zone Water Dynamics, Vadose Zone Journal, 10(1), 412–424,
500   doi:10.2136/vzj2010.0079, 2011.

501   van Genuchten, M. T.: CLOSED-FORM EQUATION FOR PREDICTING THE HYDRAULIC CONDUCTIVITY OF
502   UNSATURATED SOILS., Soil Science Society of America Journal, 44(5), 892–898, 1980.

503   Geuzaine, C. and Remacle, J.-F.: Gmsh: A 3-D finite element mesh generator with built-in pre- and post-
504   processing facilities, International Journal for Numerical Methods in Engineering, 79(11), 1309–1331,
505   doi:10.1002/nme.2579, 2009.

506   Ginsburg, H. and Laties, G. G.: Longitudinal electrical resistance of maize roots, Journal of Experimental
507   Botany, 24(6), 1035–1040, doi:10.1093/jxb/24.6.1035, 1973.

508   Hanke, M., Harrach, B. and Hyvönen, N.: Justification of point electrode models in electrical impedance
509   tomography, Math. Models Methods Appl. Sci., 21(06), 1395–1413, doi:10.1142/S0218202511005362,
510   2011.

511   Javaux, M., Schröder, T., Vanderborght, J. and Vereecken, H.: Use of a three-dimensional detailed
512   modeling approach for predicting root water uptake, Vadose Zone Journal, 7(3), 1079–1088,
513   doi:10.2136/vzj2007.0115, 2008.

514   Jougnot, D., Linde, N., Revil, A. and Doussan, C.: Derivation of soil-specific streaming potential electrical
515   parameters from hydrodynamic characteristics of partially saturated soils, Vadose Zone Journal, 11(1), 0,
516   doi:10.2136/vzj2011.0086, 2012.

517   Laloy, E., Javaux, M., Vanclooster, M., Roisin, C. and Bielders, C. L.: Electrical Resistivity in a Loamy Soil:
518   Identification of the Appropriate Pedo-Electrical Model, Vadose Zone Journal, 10(3), 1023–1033,
519   doi:10.2136/vzj2010.0095, 2011.

520   Lobet, G., Pagès, L. and Draye, X.: A Novel Image-Analysis Toolbox Enabling Quantitative Analysis of Root
521   System Architecture, Plant Physiol., 157(1), 29–39, doi:10.1104/pp.111.179895, 2011.

522   Michot, D., Benderitter, Y., Dorigny, A., Nicoullaud, B., King, D. and Tabbagh, A.: Spatial and temporal
523   monitoring of soil water content with an irrigated corn crop cover using surface electrical resistivity
524   tomography, Water Resources Research, 39(5), SBH141–SBH1420, 2003.

525   Michot, D., Thomas, Z. and Adam, I.: Nonstationary of the electrical resistivity and soil moisture
526   relationship in a heterogeneous soil system: a case study, SOIL, 2(2), 241–255, doi:10.5194/soil-2-241-
527   2016, 2016.

528   Paglis, C. M.: Application of Electrical Resistivity Tomography for Detecting Root Biomass in Coffee Trees,
529   International Journal of Geophysics, doi:10.1155/2013/383261, 2013.

530   Rossi, R., Amato, M., Bitella, G., Bochicchio, R., Ferreira Gomes, J. J., Lovelli, S., Martorella, E. and Favale,
531   P.: Electrical resistivity tomography as a non-destructive method for mapping root biomass in an
532   orchard, European Journal of Soil Science, 62(2), 206–215, doi:10.1111/j.1365-2389.2010.01329.x, 2011.

533   Schöberl, J.: An advancing front 2D/3D-mesh generator based on abstract rules, Computing and
534   Visualization in Science, 1(1), 41–52, doi:10.1007/s007910050004, 1997.

535   Srayeddin, I. and Doussan, C.: Estimation of the spatial variability of root water uptake of maize and
536   sorghum at the field scale by electrical resistivity tomography, Plant Soil, 319(1–2), 185–207,
537   doi:10.1007/s11104-008-9860-5, 2009.

538   Tournier, P.-H., Hecht, F. and Comte, M.: Finite Element Model of Soil Water and Nutrient Transport with
539   Root Uptake: Explicit Geometry and Unstructured Adaptive Meshing, Transport in Porous Media, 106(2),
540   487–504, doi:10.1007/s11242-014-0411-7, 2015.

541   Vanella, D., Cassiani, G., Busato, L., Boaga, J., Barbagallo, S., Binley, A. and Consoli, S.: Use of small scale
542   electrical resistivity tomography to identify soil-root interactions during deficit irrigation, Journal of
543   Hydrology, 556, 310–324, doi:10.1016/j.jhydrol.2017.11.025, 2018.

544   Waxman, M. H. and Smits, L. J. M.: Electrical Conductivities in Oil-Bearing Shaly Sands, SPE-1863-A,
545   doi:10.2118/1863-A, 1968.

546   Werban, U., Al Hagrey, S. A. and Rabbel, W.: Monitoring of root-zone water content in the laboratory by
547   2D geoelectrical tomography, Journal of Plant Nutrition and Soil Science, 171(6), 927–935,
548   doi:10.1002/jpln.200700145, 2008.

549   Whalley, W. R., Binley, A., Watts, C. W., Shanahan, P., Dodd, I. C., Ober, E. S., Ashton, R. W., Webster, C.
550   P., White, R. P. and Hawkesford, M. J.: Methods to estimate changes in soil water for phenotyping root
551   activity in the field, , doi:10.1007/s11104-016-3161-1, 2017.

552   Wilderotter, O.: An adaptive numerical method for the Richards equation with root growth, Plant and
553   Soil, 251(2), 255–267, doi:10.1023/A:1023031924963, 2003.

554   Wunderlich, T., Petersen, H., al Hagrey, S. A. and Rabbel, W.: Pedophysical models for resistivity and
555   permittivity of partially water-saturated soils, Vadose Zone Journal, 12(4), doi:10.2136/vzj2013.01.0023,
556   2013.

557   Zenone, T., Morelli, G., Teobaldelli, M., Fischanger, F., Matteucci, M., Sordini, M., Armani, A., Ferrè, C.,
558   Chiti, T. and Seufert, G.: Preliminary use of ground-penetrating radar and electrical resistivity
559   tomography to study tree roots in pine forests and poplar plantations, Functional plant biology FPB
560   [online] Available from: http://agris.fao.org/agris-search/search.do?recordID=US201301559026
561   (Accessed 14 September 2017), 2008.

562

563

564

565

566

567

568   **Tables:**

569

	θr [cm^3 cm^{-3}]	θs[cm^3 cm^{-3}]	a [1/cm]	n	Ks [cm/day]	λ
Sand	0	0.35	0.05	2	100.24	0.5
Loam	0.078	0.435	0.036	1.56	25	0.6

570

571   Table 1: Soil hydraulic properties. θr: Residual water content, θs: Saturated water content, a , n

572   and λ: shape parameters in van Genuchten-Mualem equations, Ks: saturated soil hydraulic

573   conductivity.

574

575

576

577

578

579

580

581

582

583

584

585

586

587

588

a) Sand without roots	Time:	Day 5	Day 10	Day 15	Day 18	Day 22
	σ_{bulkZ} [S/m]	0.0127	0.0074	0.0041	0.0015	0.0002
	σ_{bulkX} [S/m]	0.0215	0.0144	0.0106	0.0064	0.0012
	AF	1.68	1.93	2.58	4.26	6.24
b) Sand with roots	σ_{bulkZ} [S/m]	0.0128	0.0077	0.0045	0.0018	0.0002
	σ_{bulkX} [S/m]	0.0215	0.0144	0.0108	0.0066	0.0012
	AF	1.67	1.88	2.39	3.73	6
c) Loam without roots	σ_{bulkZ} [S/m]	0.0568	0.0449	0.0370	0.0279	0.0166
	σ_{bulkX} [S/m]	0.0594	0.0482	0.0417	0.0337	0.0190
	AF	1.04	1.07	1.12	1.19	1.14
d) Loam with roots	σ_{bulkZ} [S/m]	0.0566	0.0447	0.0369	0.0281	0.0170
	σ_{bulkX} [S/m]	0.0593	0.0481	0.0414	0.0334	0.0194
	AF	1.04	1.07	1.12	1.19	1.14

589

Table 2: Effective electrical conductivity in [S/m] and anisotropy factor at rhizotron scale computed using simulated plate electrodes at boundaries.

592

593

594

595 **Figures:**

596
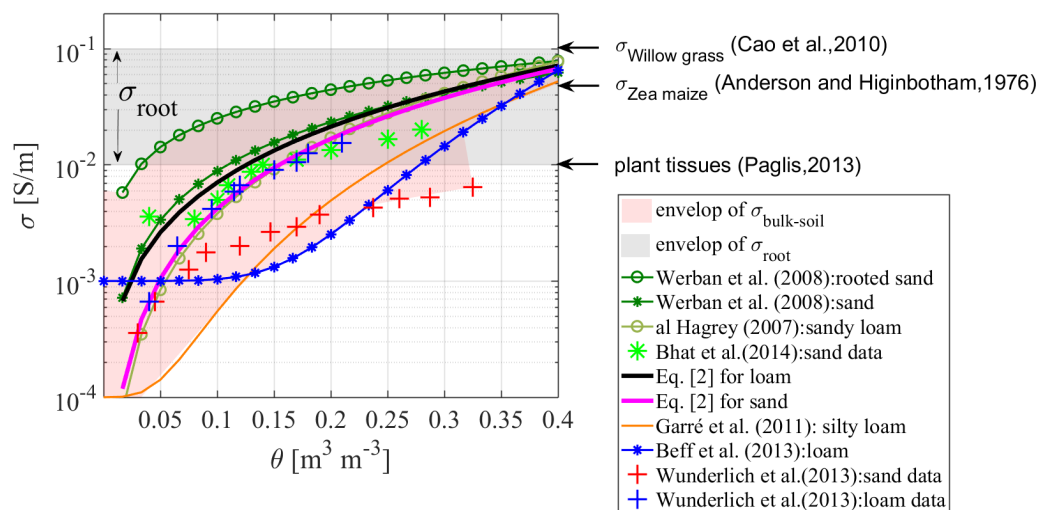
597

598 Figure 1. Comparison of soil and root electrical conductivity. The envelops of σ_{soil} (some with

599 and some without roots) and σ_{root} are shown as shaded areas.

600

601

602

603
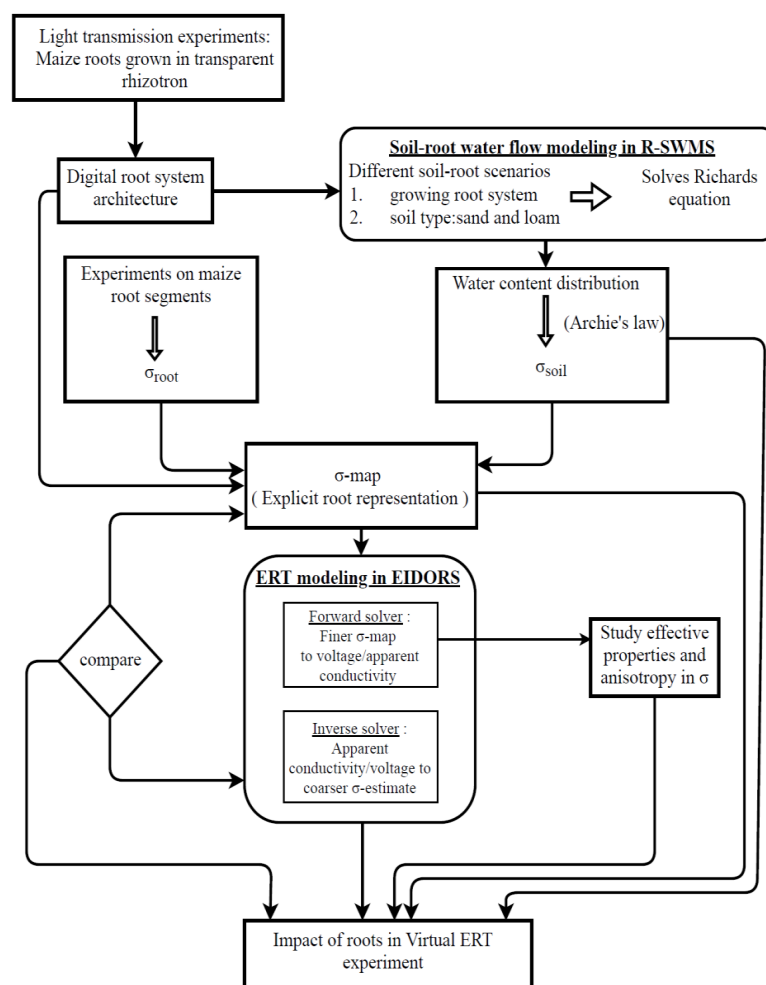
Figure 2: Flow chart for the simulation of Virtual Rhizotron drying experiment. First, a simulation of root water uptake and root growth of a maize plant in a rhizotron is run with a soil-plant water flow model (RSWMS, Javaux et al., 2008), which generates maps of soil water distribution (θ) and of root architecture evolution. Then these distributions are transformed into detailed electrical conductivity (σ) maps through bio/pedo-physical relations. Third, these distributions are used to simulate a virtual ERT measurement and inversion scheme to get a coarser distribution of σ estimates (see text for further details).

611
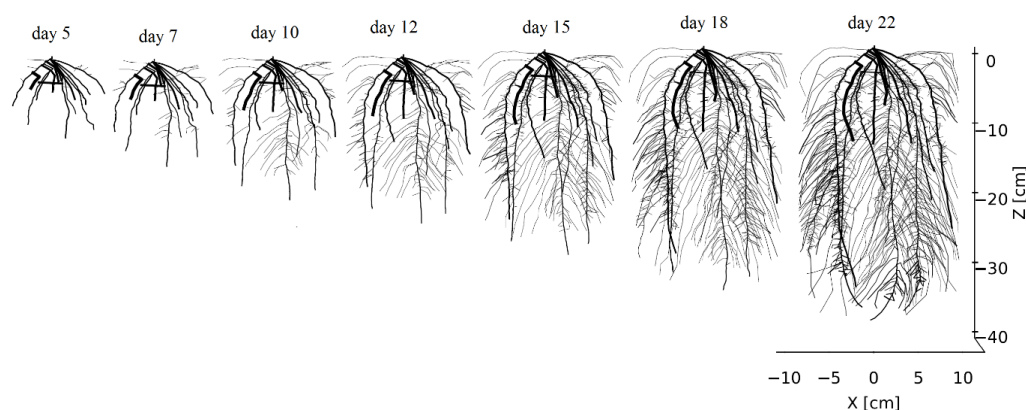
Figure 3: root architectural evolution shown at different times.

613
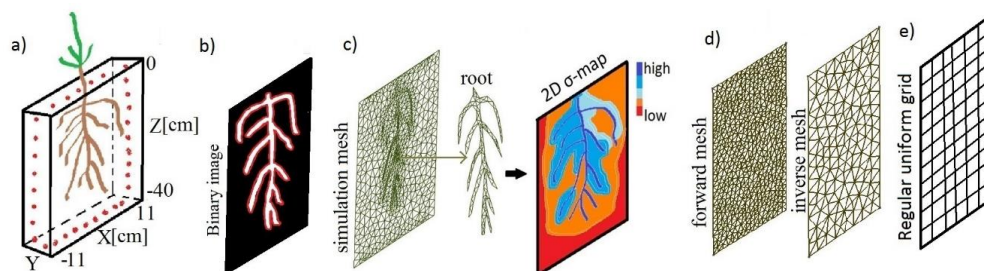
Figure 4: a) Virtual rhizotron schematic, b) binary image of schematic root architecture used to generate mesh. The red region represents the spline curve that envelops the root surface. c) Simulation model (SMDL): simulation mesh with explicit root architecture and schematic conductivity distribution map, d) forward model (FMDL): forward and inverse mesh, and e) regular uniform grid used to simulate Richards' equation.

619

620

621
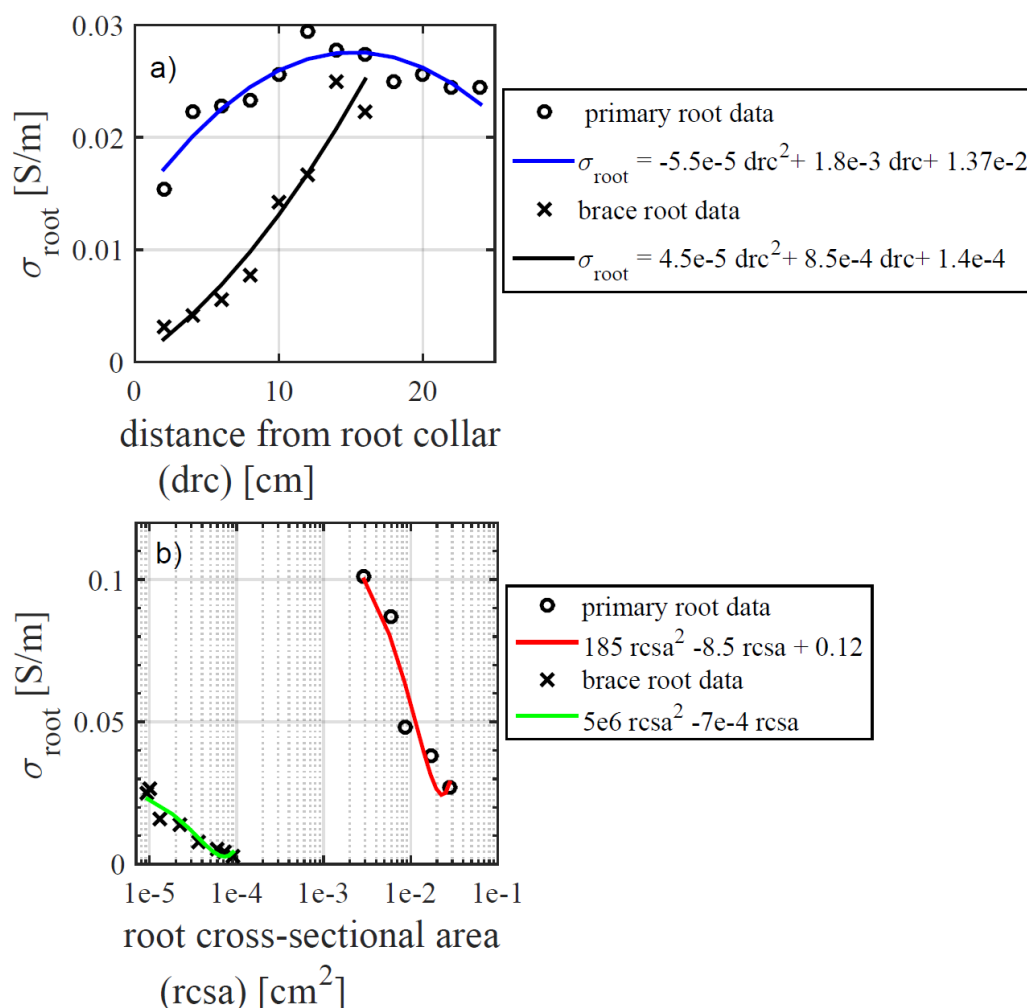
Figure 5: Measurement data on Maize roots a) σ_{root} vs distance from root collar, b) σ_{root} vs root

cross sectional area. The quadratic fit is shown as solid line while measurement data is

represented at discrete locations as circles (primary root) and crosses (brace root). The blue curve
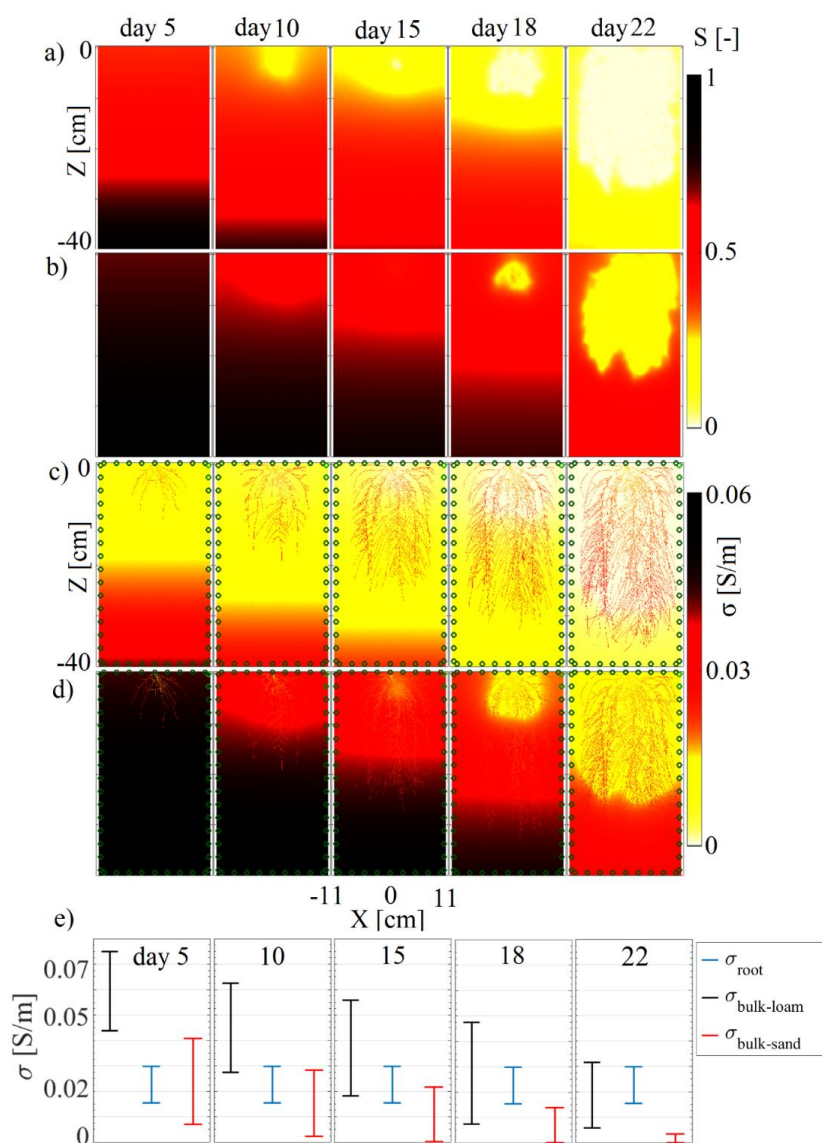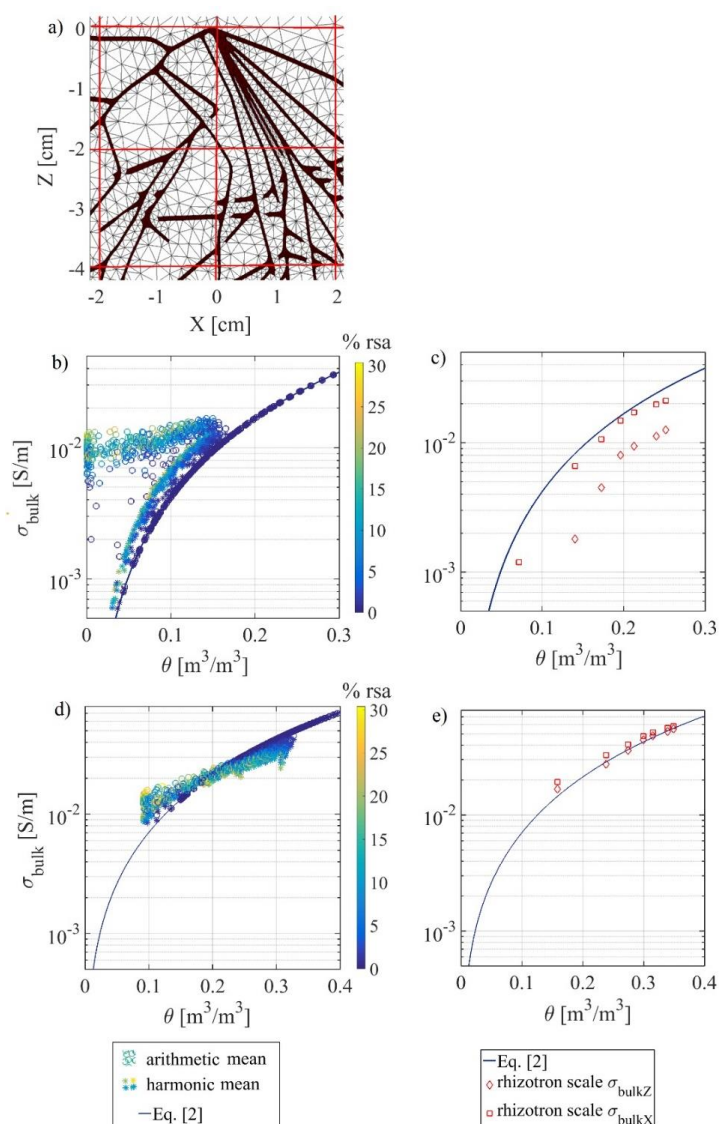
in Figure 5a is the data used in simulation model.

Figure 6: Volumetric water saturation distribution in a) sand and b) loam, and its corresponding σ-maps in c) sand and d) loam, e) variability of σ in the rhizotron at different times. The vertical bars at various times represent the minimum and maximum value of σ, respectively.

Figure 7: a) A section of the SMDL mesh with averaging blocks shown in red squares. The root elements are in brown color, b) Comparison of Eq. [2] with block-wise averaged quantities ($<\sigma_{bulk}>$ vs. $<\theta>$) in sand, c) Comparison of Eq. [2] with rhizotron scale effective bulk property in sand, d) Comparison of Eq. [2] with block-wise averaged quantities ($<\sigma_{bulk}>$ vs. $<\theta>$) in loam, c) Comparison of Eq. [2] with rhizotron scale effective bulk property in loam.

637
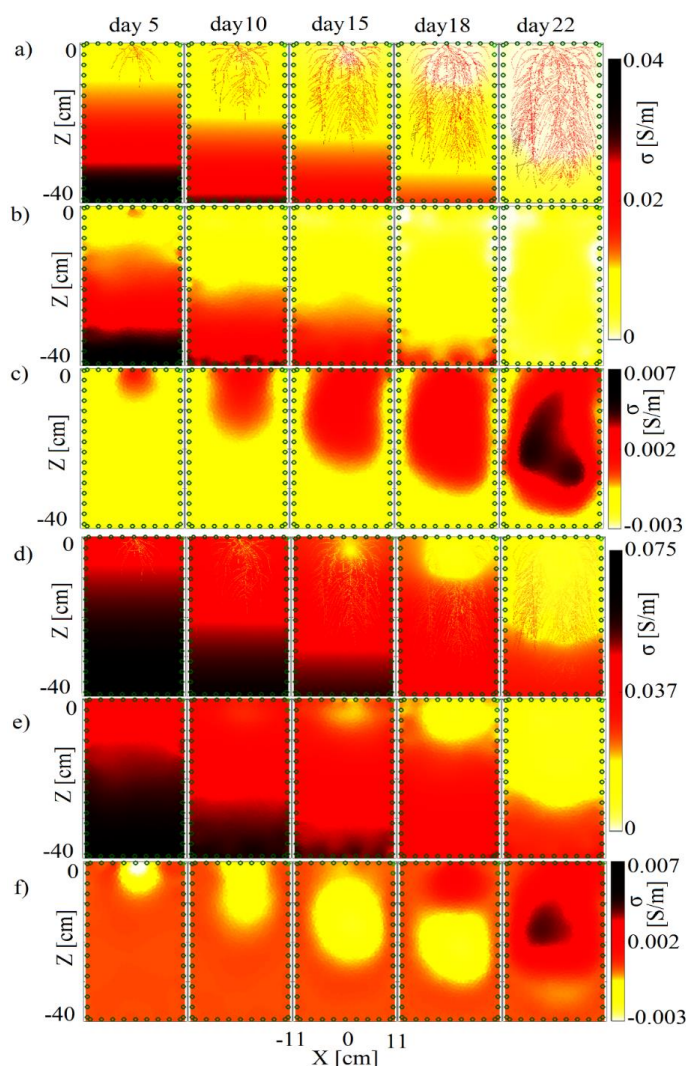
Figure 8: Sand: a) detailed electrical conductivity map of maize root at different times; b)
tomography inversion with the root conductivity included in the forward model; c) difference
between the inversions results with and without root conductivity accounted for in the forward
model. Green circles represent the electrode positions. Loam: d) Conductivity map of maize
root at different time; e) tomography inversion with the root conductivity included in the
forward model; f) difference between the inversions results with and without root conductivity
in the forward model.

645
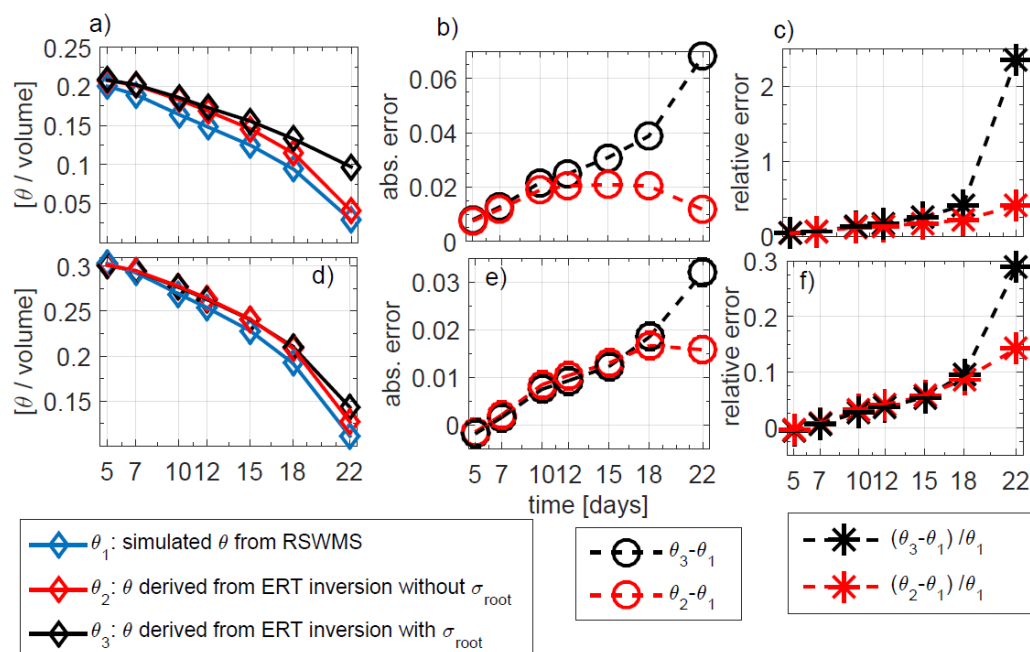
Figure 9: a) Comparison of normalized volume averaged water content, obtained from simulated

SWC (denoted as θ_1) and ERT imaging without and with inclusion of σ_{root} denoted by θ_2 and θ_3,

respectively as a function of different root growth time in sand, b) Absolute error between

(θ_1,θ_3) and (θ_1,θ_2), c) relative error between (θ_1,θ_3) and (θ_1,θ_2). Figures 9 (d,e,f) same as 9

(a,b,c) but in loam medium.

651